

Journal of Materials Chemistry C

Accepted Manuscript



This is an *Accepted Manuscript*, which has been through the Royal Society of Chemistry peer review process and has been accepted for publication.

Accepted Manuscripts are published online shortly after acceptance, before technical editing, formatting and proof reading. Using this free service, authors can make their results available to the community, in citable form, before we publish the edited article. We will replace this *Accepted Manuscript* with the edited and formatted *Advance Article* as soon as it is available.

You can find more information about *Accepted Manuscripts* in the [Information for Authors](#).

Please note that technical editing may introduce minor changes to the text and/or graphics, which may alter content. The journal's standard [Terms & Conditions](#) and the [Ethical guidelines](#) still apply. In no event shall the Royal Society of Chemistry be held responsible for any errors or omissions in this *Accepted Manuscript* or any consequences arising from the use of any information it contains.

ARTICLE

Significance of ions with an ordered arrangement for enhancing the electron injection/extraction in polymer optoelectronic devices

Cite this: DOI: 10.1039/x0xx00000x

Received 00th January 2012,
Accepted 00th January 2012

DOI: 10.1039/x0xx00000x

www.rsc.org/

Chen-Hao Wu,^a Chih-Yun Chin,^a Tsan-Yao Chen,^b Tzung-Fang Guo,^{c,d} Chih-Hao Lee,^b Tsang-Lang Lin,^b Alex K.-Y. Jen^e and Ten-Chin Wen^{*a,d}

We demonstrate the significance of ions with an ordered arrangement for enhancing the electron injection in polymer light-emitting diodes (PLEDs) and the electron extraction in polymer solar cells (PSCs) by using tetraoctylammonium bromide (TOAB) as a model compound. The spin-coated films of TOAB are prepared on the active layers of both PLEDs and PSCs without any annealing (TOAB-No) as well as with the annealing at 60 °C (TOAB-60) and 100 °C (TOAB-100). Subsequently, they are investigated by atomic force microscopy (AFM) and synchrotron X-ray diffraction (XRD) as well as simultaneously employed as the interfacial layers in PLEDs and PSCs. The AFM results show that the active layers are well covered with TOAB-No and TOAB-100, but poorly covered with TOAB-60 due to the formation of large islands. The XRD results show that TOAB-No and TOAB-60 are polycrystalline with the (002) lattice planes parallel to the surface of the active layers while TOAB-100 presents amorphous. Of note, the electron injection in PLEDs and the electron extraction in PSCs are significantly enhanced using TOAB-No and TOAB-60, but both are worsened using TOAB-100. Evidently the enhanced electron injection/extraction is mainly attributed to the ordered arrangement of ions in the TOAB crystals. This study prompts us that with an order arrangement of ions, all ionic compounds should be excellent for enhancing the electron injection/extraction in polymer optoelectronic devices.

Introduction

Polymer light-emitting diodes (PLEDs) and polymer solar cells (PSCs) have attracted considerable attention due to their potential for realizing lightweight, flexible, and large-area devices.^{1,2} To achieve high-performance PLEDs and PSCs, the energy level alignment at the active layer-electrode interface is necessary for efficient charge transfer.^{3,4} Conventionally, low work function metals such as Ca and Ba are used as cathodes to ensure the efficient electron injection in PLEDs and the efficient electron extraction in PSCs. However, they are sensitive to moisture and oxygen, which undermines their use for practical applications. Stable metals such as Al, Ag, and Au have been used as cathodes, but their high work function mismatches with the lowest unoccupied molecular orbital (LUMO) of the active layer. Therefore, an interfacial layer must be employed to decrease the energy level difference between the LUMO of the active layer and the work function of the metal cathode for efficient electron injection/extraction.^{5,6}

Conjugated polyelectrolytes (CPEs) are promising materials as solution-processed interfacial layers in PLEDs and PSCs.⁶⁻⁹ Their ionic pendant groups ensure the solubility in polar solvents, and therefore allow the solution-based fabrication of multilayer devices. The excellent performance of PLEDs and PSCs with CPEs is attributable to the interfacial dipole between

the active layer and the Al cathode.¹⁰ On the other hand, the ion motion in CPEs leads to a redistribution of the internal electric field and a long response time of PLEDs.¹¹⁻¹³ Conjugated polymeric zwitterions (CPZs) have attracted much attention due to their chemical structure comprising immobile ions.¹⁴⁻¹⁸ The CPZs significantly boost the electron injection in PLEDs, lead to the short response time of PLEDs, and also enhance the electron extraction in PSCs. In fact, the conjugated system of an interfacial layer is not essential to enhance the electron injection while the ions are important. Recently, small-molecule zwitterions without conjugated systems are spin-coated on electroluminescent polymers to ensure the efficient electron injection in high-performance PLEDs.¹⁹ When they are spin-coated on the active layer of PSCs, the electron extraction in PSCs is not improved. The assembly of these small-molecule zwitterions may be affected by the underlying substrate, resulting in the different arrangement of ions. The proper arrangement of ions within an interfacial layer should be essential to enhance the electron injection/extraction.

Tetra-*n*-alkyl ammonium bromides (TAABs), commonly used as the ionic functionalities of CPEs, have been used as solution-processed interfacial layers in high-performance PLEDs and PSCs.^{20,21} They significantly enhance the performance of PLEDs with Al, Ag, and Au cathodes as well as lead to the short response time of PLEDs. Additionally, they

enhance the short-circuit current density (J_{SC}), open-circuit voltage (V_{OC}), and fill factor (FF), resulting in the high power conversion efficiency (PCE) of PSCs. The TAABs crystallize as stacked monolayers with an “ionic plane” consisting of an array of bromide ions (Br^-) and the positively charged N atoms (N^+) in the middle of each layer.²² Due to the flexible n-alkyl chains, they show a multi-step fusion behavior,²³ which provides the opportunity to change their arrangement of ions via annealing. In this study, we demonstrate that the arrangement of ions in an interfacial layer dramatically affects the performance of PLEDs and PSCs. In order to directly observe the arrangement of ions, tetraoctylammonium bromide (TOAB) is chosen as a model compound to prepare the interfacial layers possessing the different arrangement of ions. The ethanol solution of TOAB (2 mg ml^{-1}) was spin-coated atop the active layer without any annealing to complete the interfacial layer denoted as TOAB-No. Polyfluorene Green B (G-PF) was used as the active layer of PLEDs and the blend of poly(3-hexylthiophene) and [6,6]-phenyl-C61 butyric acid methyl ester (P3HT:PCBM) was used as the active layer of PSCs.^{24,25} TOAB-No was subsequently annealed at 60°C and 100°C to complete the interfacial layers denoted as TOAB-60 and TOAB-100, respectively. The results demonstrate that the ordered arrangement of ions makes the interfacial layer of TOAB effective in enhancing the electron injection in PLEDs and the electron extraction in PSCs.

Results and Discussion

The surface morphology of TOAB-No, TOAB-60, and TOAB-100 atop G-PF was first explored by atomic force microscopy (AFM). The results are shown in Fig. 1a. The TOAB-No and TOAB-100 surfaces are smooth and have the root mean square (rms) roughness of 1.79 nm and 4.84 nm, respectively. On the other hand, the TOAB-60 surface is really rough and has the rms roughness of 8.12 nm due to the large islands. The corresponding AFM phase images (Fig. 1b) clearly display that TOAB-No and TOAB-100 are continuous films fully covering the underlying G-PF, whereas TOAB-60 is a discontinuous film covering only a 46.8% area of G-PF. Evidently the octyl chains of TOAB are long enough to ensure a well adhesion with the hydrophobic G-PF during the spin-coating process. The different surface morphology is attributable to the reassembly of TOAB molecules occurring at the transition temperature (50°C) and the melting point (101°C).²³

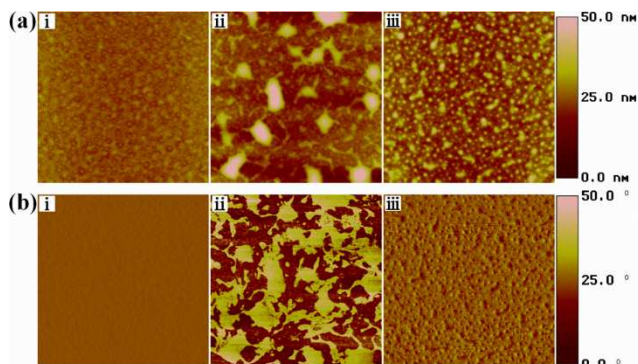


Fig. 1 (a) AFM topography images and (b) AFM phase images of i) TOAB-No, ii) TOAB-60, iii) TOAB-100 atop G-PF. Scale: $10 \mu\text{m} \times 10 \mu\text{m}$.

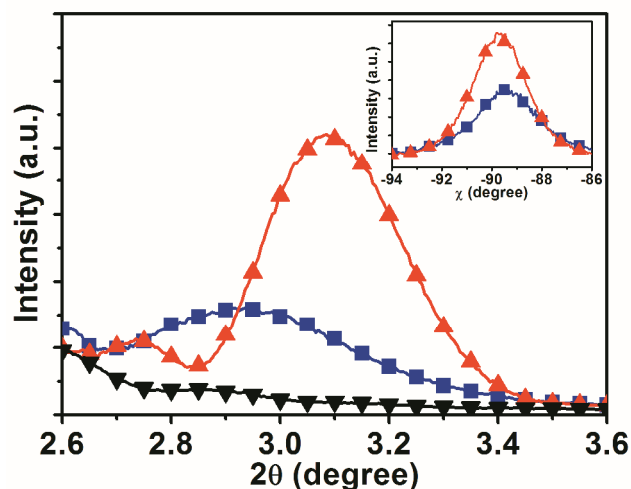


Fig. 2 Synchrotron XRD patterns of the samples with configurations as ITO/PEDOT:PSS/G-PF/TOAB-No (■), ITO/PEDOT:PSS/G-PF/TOAB-60 (▲), ITO/PEDOT:PSS/G-PF/TOAB-100 (▼). Inset: the rocking curves for the (002) peak of TOAB.

In order to further understand the molecular assembly of TOAB-No, TOAB-60, and TOAB-100 atop G-PF, samples were examined by synchrotron X-ray diffraction (XRD). The corresponding results are shown in Fig. 2. Crystals in the TOAB powder show the lamellar structure where the preferential arrangement of TOAB molecules is the C2/c symmetry along (002) lattice planes with an interplanar spacing of 18.6 \AA .^{20,22} In the XRD pattern of indium tin oxide (ITO)/poly(3,4-ethylenedioxythiophene)-poly(styrenesulfonate) (PEDOT:PSS)/G-PF/TOAB-No, the peak originates from the (002) lattice planes of TOAB crystals and corresponds to a d -spacing of 19.8 \AA . This larger d -spacing than that observed in TOAB powder is attributable to the residual stress originated from the out of equilibrium chain conformation in the spin-coated film.²⁶ The average grain size of crystals, which is estimated by the full width at half maximum (FWHM) of a peak, is 16.0 nm . Based on the smooth surface of TOAB-No, we speculate that TOAB-No is thick enough (at least 10.0 nm) to accommodate the crystals with average grain size of 16.0 nm . In the XRD pattern of ITO/PEDOT:PSS/G-PF/TOAB-60, the peak corresponds to a smaller d -spacing (19.0 \AA) as well as has a narrower FWHM and a higher intensity than that in the XRD pattern of ITO/PEDOT:PSS/G-PF/TOAB-No. The small d -spacing may be due to the relaxation of residual stress

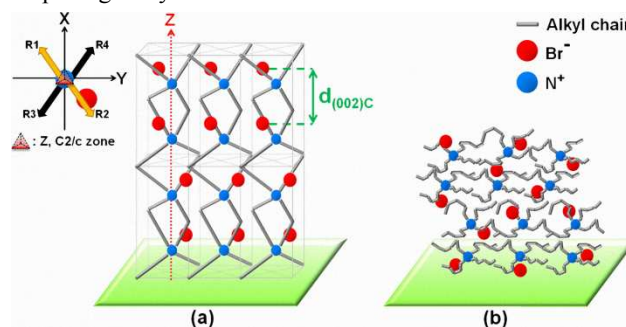


Fig. 3 (a) The ordered arrangement between Br^- and N^+ in TOAB-No and TOAB-60. (b) The disordered arrangement between Br^- and N^+ in TOAB-100.

Table 1 The detailed performance parameters of PLEDs with Al, TOAB-No/Al, TOAB-60/Al, and TOAB-100/Al cathodes

Cathode	V_{J-on} [V]	V_{L-on} [V]	Current Density ^a [mA cm ⁻²]	Luminance ^a [cd m ⁻²]	Luminance Efficiency ^b [cd A ⁻¹]
Al	1.5	3.4	47.8	129.7	0.4
TOAB-No/Al	1.9	2.1	375.5	35289	13.8
TOAB-60/Al	1.9	2.1	308.8	25341	10.9
EA TOAB-60/Al	1.9	2.1	659.8	54147	10.9
TOAB-100/Al	-	-	0.9	16.4	-

^a At the bias of 7.0 V. ^b At 20.0 mA cm⁻². EA: Effective Area.

by the reassembly of TOAB molecules. The narrow FWHM clearly shows that the average grain size of crystals is increased from 16.0 nm to 19.6 nm via the annealing at 60 °C. The increase in the average grain size of crystals is responsible for the high peak intensity. To further confirm the orientation of crystals in TOAB-No and TOAB-60, the peak intensity is monitored with two samples tilted in a few degrees along the chi dimension. In the corresponding rocking curves (the inset of Fig. 2), the maximal peak intensity is located nearly at $\chi = -90^\circ$. It demonstrates that there is a preferential orientation of crystals in TOAB-No and TOAB-60: the (002) lattice planes of TOAB crystals are parallel to (the *d*-spacing are normal to) the hydrophobic surface of G-PF (Fig. 3a). In this preferential arrangement of TOAB molecules, the ordered arrangement between Br⁻ and N⁺ provides the net interfacial dipole pointing toward G-PF. The rocking curve for ITO/PEDOT:PSS/G-PF/TOAB-60 has the narrower FWHM than that for

ITO/PEDOT:PSS/G-PF/TOAB-No. It indicates that the ordering of TOAB crystals also become more converged toward the preferential orientation via the annealing at 60 °C, besides the increase in the average grain size of crystals. Therefore, we expect that TOAB-60 provides the larger interfacial dipole pointing toward G-PF than TOAB-No. On the other hand, there is no Bragg diffraction peak in the XRD pattern of ITO/PEDOT:PSS/G-PF/TOAB-100. It depicts that the annealing at 100 °C ruins the TOAB crystals and results in the amorphous TOAB-100 where Br⁻ and N⁺ are disorderly arranged and consequently the molecular dipoles offset each other (Fig. 3b).

PLEDs with Al, TOAB-No/Al, TOAB-60/Al, and TOAB-100/Al cathodes were used to explore the relationship between the arrangement of ions and the electron injection. Fig. 4a shows the current density-voltage-luminance (*J-V-L*) characteristics of four devices. Owing to the very low current density and luminance for the device with the TOAB-100/Al cathode, Fig. 4b only shows the luminance efficiency vs. current density for devices with Al, TOAB-No/Al, and TOAB-60/Al cathodes. Table 1 summarizes their detailed performance parameters. In the device with an Al cathode, the current turn-on voltage (V_{J-on}) is 1.5 V and the light turn-on voltage (V_{L-on}) is 3.4 V. The energy level difference between the LUMO of G-PF (-3.0 eV) and the work function of Al (-4.3 eV), the electron injection barrier, is much larger than that between the highest occupied molecular orbital of G-PF (-5.5 eV) and the work function of PEDOT:PSS (-5.1 eV), the hole injection barrier.^{24,5} Accordingly, holes can be injected from the ITO/PEDOT:PSS anode into G-PF at 1.5 V, whereas electrons cannot be injected from the Al cathode into G-PF and then recombine with holes

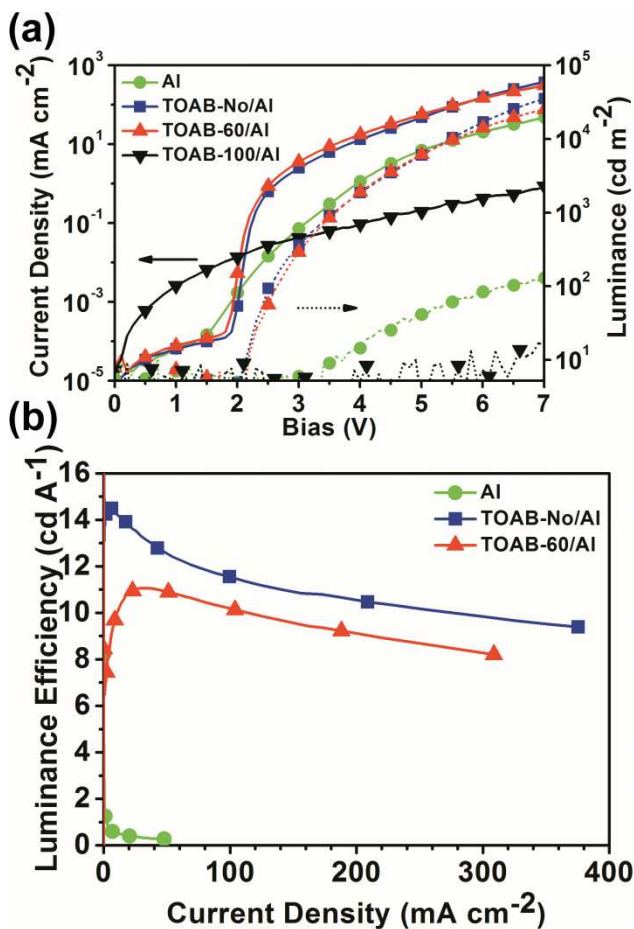


Fig. 4 (a) *J-V-L* characteristics of PLEDs with Al, TOAB-No/Al, TOAB-60/Al, and TOAB-100/Al cathodes. (b) The luminance efficiency vs. current density for devices with Al, TOAB-No/Al, and TOAB-60/Al cathodes.

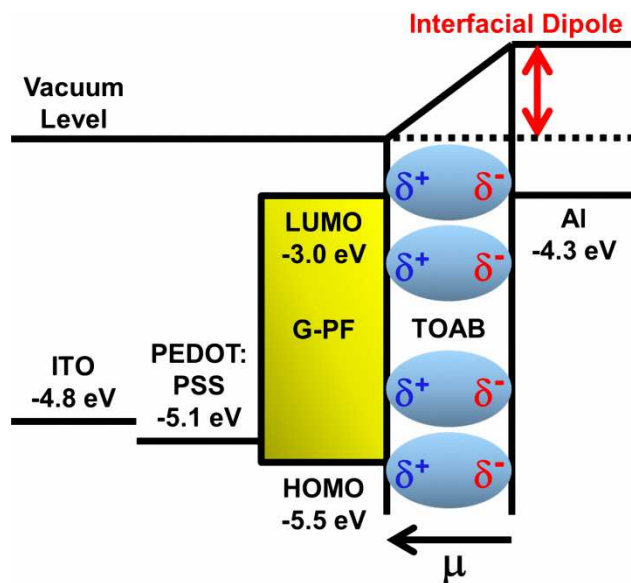


Fig. 5 Energy level diagram for the PLED with the electron injection layer of TOAB.

to emit the light until 3.4 V. This unbalanced injection of holes and electrons is responsible for both the low current density and the luminance (47.8 mA cm^{-2} and 129.7 cd m^{-2} at the bias of 7.0 V) as well as the low luminance efficiency (0.4 cd A^{-1} at 20.0 mA cm^{-2}). Devices with TOAB-No/Al and TOAB-60/Al cathodes show the much higher current density, luminance, and luminance efficiency as well as the lower V_{L-on} than the device with an Al cathode. Notice that the large islands of TOAB-60 do not adversely affect the device performance. These improvements are attributable to the interfacial dipole toward G-PF introduced by TOAB-No and TOAB-60. The interfacial dipole is presumed to elevate the vacuum level of the Al cathode, and therefore decreases the energy level difference between the LUMO of G-PF and the work function of the Al cathode (Fig. 5).²⁷ Consequently, the electron injection from the Al cathode to G-PF is significantly enhanced. The difference between V_{J-on} and V_{L-on} is only 0.2 V in devices with TOAB-No/Al and TOAB-60/Al cathodes. It indicates that the balanced injection of holes and electrons is accomplished and contributes to their high luminance efficiency. Recall that TOAB-60 only covers the 46.8% area of G-PF so that it cannot entirely protect G-PF from the formation of metal-induced quenching sites during thermal evaporation of the Al cathode.²⁸ Thus the device with the TOAB-60/Al cathode shows the lower luminance efficiency than the device with the TOAB-No/Al cathode. Notice that both the V_{L-on} and the V_{J-on} in the device with the TOAB-60/Al cathode are the same as those in the device with the TOAB-No/Al cathode. Since the G-PF surface is fully covered with TOAB-No, we suppose that the electron injection in the device with the TOAB-60/Al cathode occurs only in the 46.8% area of G-PF in contact with TOAB-60. Therefore, the current density and the luminance in the device with the TOAB-60/Al cathode are calibrated by considering the effective area and shown in Table 1. Interestingly, the effective values are much higher than those in the device with the TOAB-No/Al cathode. It is attributable to the larger interfacial dipole introduced by TOAB-60 than TOAB-No. It also suggests that the electron injection can be further enhanced by improving the preferential arrangement of TOAB molecules. The four alkyl chains in the tetra-*n*-alkyl ammonium cation prevent an anion from approaching closely to N^+ , which provides quaternary ammonium salts the large dipole ($\gg 11 \text{ D}$).²⁹ Accordingly, we infer that the multilayer structure of TOAB-No and TOAB-60 introduces the interfacial dipole large enough to ensure the ohmic contact between G-PF and the Al cathode. It is the possible reason that the same V_{L-on} and V_{J-on} are observed in the devices with TOAB-No/Al and TOAB-60/Al cathodes. On the other hand, the device with the TOAB-100/Al cathode doesn't show the diode characteristics and has a very low current density (0.9 mA cm^{-2} at the bias of 7.0 V). Evidently TOAB-100 just acts an insulating layer to block the electron injection since it cannot provide any interfacial dipole. Although TOAB-No and TOAB-100 have the similar surface morphology, they have the opposite effect on the electron injection. It clearly demonstrates that the ordered arrangement between Br^- and N^+ make the interfacial layer of TOAB effective in enhancing the electron injection.

Several small molecules containing ions are used to improve the electron injection in PLEDs.³⁰⁻³⁴ However, they have not been used to enhance the electron extraction in PSCs. In our previous study, we demonstrate that TOAB significantly enhances the electron extraction in the PSCs with Al, Ag, and Au cathodes.²¹ Herein we also show the ordered arrangement between Br^- and N^+ is necessary for the efficient electron

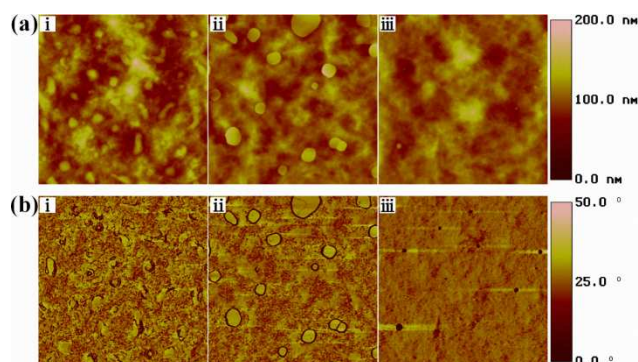


Fig. 6 (a) AFM topography images and (b) AFM phase images of i) TOAB-No, ii) TOAB-60, iii) TOAB-100 atop P3HT:PCBM. Scale: $10 \mu\text{m} \times 10 \mu\text{m}$.

extraction between PCBM and an Al cathode. The behavior of TOAB molecules on the P3HT:PCBM surface is similar to that on the G-PF surface (Fig. 6a and 6b). The P3HT:PCBM surface is well covered with TOAB-No and TOAB-100, but it is poorly covered with TOAB-60 due to the formation of large islands. Fig. 7 shows the synchrotron XRD patterns of three samples. It is clear that TOAB molecules nucleate on the P3HT:PCBM surface and grow into the crystals with the average grain size of 66.1 nm via the spin-coating process. Moreover, the average grain size of TOAB crystals is increased from 66.1 nm to 88.1 nm via the annealing at 60°C . Furthermore, the corresponding rocking curves (the inset of Fig. 7) indicate that the (002) lattice planes of these TOAB crystals are parallel to the (*d*-spacing are normal to) the hydrophobic surface of P3HT:PCBM. The rocking curve for ITO/PEDOT:PSS/P3HT:PCBM/TOAB-60 has the broader FWHM than that for ITO/PEDOT:PSS/P3HT:PCBM/TOAB-No. It indicates that the ordering of TOAB crystals become more diverged from the preferential orientation via the annealing at 60°C . Therefore, the peak shows a lower intensity even though the average grain size of TOAB crystals is increased. Consequently, TOAB-60 provides the smaller interfacial dipole pointing toward

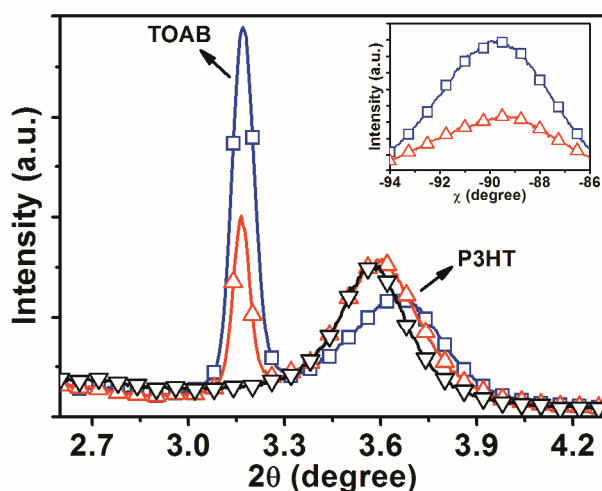


Fig. 7 Synchrotron XRD patterns of the samples with configurations as ITO/PEDOT:PSS/P3HT:PCBM/TOAB-No (□), ITO/PEDOT:PSS/P3HT:PCBM/TOAB-60 (△),

ITO/PEDOT:PSS/P3HT:PCBM/TOAB-100 (∇). Inset: the rocking curves for the (002) peak of TOAB.

atop P3HT:PCBM also show the amorphous character the same as TOAB-100 atop G-PF. Another peak observed in the XRD patterns corresponds to the interchain spacing in P3HT associated with the interdigitated alkyl chains.³⁵ Evidently the crystallinity of P3HT is improved via the annealing processes, which is the possible reason for the divergence from the preferential orientation of TOAB crystals.

PSCs with Al, TOAB-No/Al, TOAB-60/Al, and TOAB-100/Al cathodes were used to explore the relationship between the arrangement of ions and the electron extraction. Fig. 8a and 8b shows the J - V characteristics of all four devices under air mass 1.5 global (AM 1.5 G) illumination of 100 mW cm^{-2} and in the dark, respectively. The detailed performance parameters are tabulated in Table 2. The energy level difference between the LUMO of PCBM (-3.9 eV)³⁶ and the work function of the Al cathode (-4.3 eV) is responsible for the poor device performance as well as the large series resistance (R_S) in the device with an Al cathode. The interfacial dipole pointing toward P3HT:PCBM is presumed to decrease the energy level difference between the LUMO of PCBM and the work function of the Al cathode, facilitating the electron extraction.²⁷ Thus the device with the TOAB-No/Al cathode shows the higher V_{OC} , FF, and J_{SC} as well as much lower R_S than the device with an Al cathode. In the device with the TOAB-60/Al cathode, the V_{OC} is lower and the R_S is higher than those in the device with the TOAB-No/Al cathode. Besides, the device with the TOAB-60/Al cathode also shows the lower V_{J-on} than the device with

TOAB-60/Al, and TOAB-100/Al cathodes (a) under AM 1.5 G illumination of 100 mW cm^{-2} and (b) in the dark.

Table 2 The detailed performance parameters of PSCs with Al, TOAB-No/Al, TOAB-60/Al, and TOAB-100/Al cathodes

Cathode	V_{oc} [V]	J_{sc} [mA cm^{-2}]	FF	PCE [%]	R_S [$\Omega \text{ cm}^2$]
Al	0.42	10.53	0.48	2.14	14.04
TOAB-No/Al	0.58	10.63	0.64	3.97	1.42
TOAB-60/Al	0.56	10.44	0.53	3.10	1.57
TOAB-100/Al	0.34	8.73	0.28	0.84	60.67

the TOAB-No/Al cathode (Fig. 8b). These differences are attributable to the smaller built-in potential in the device with the TOAB-60/Al cathode than the TOAB-No/Al cathode since TOAB-60 provides the smaller interfacial dipole than TOAB-No.^{37,38} On the other hand, the amorphous TOAB-100 acts an insulating layer to block electron extraction, resulting in the low V_{OC} , FF, and J_{SC} as well as the high R_S . This speculation is also supported by the very poor diode characteristics of the device with the TOAB-100/Al cathode in the dark (Fig. 8b). Although the improved crystallinity of P3HT leads to the high J_{SC} and FF,³⁵ this effect is offset by the annealing effect of TOAB. Therefore, we observe that both the J_{SC} and FF are decreased with the increase in the annealing temperature. Due to the poor coverage of TOAB-60, the lower J_{SC} and FF in the device with the TOAB-60/Al cathode than with the TOAB-No/Al cathode should be attributable to the metal-induced quenching sites near the P3HT:PCBM/Al interface.³⁹

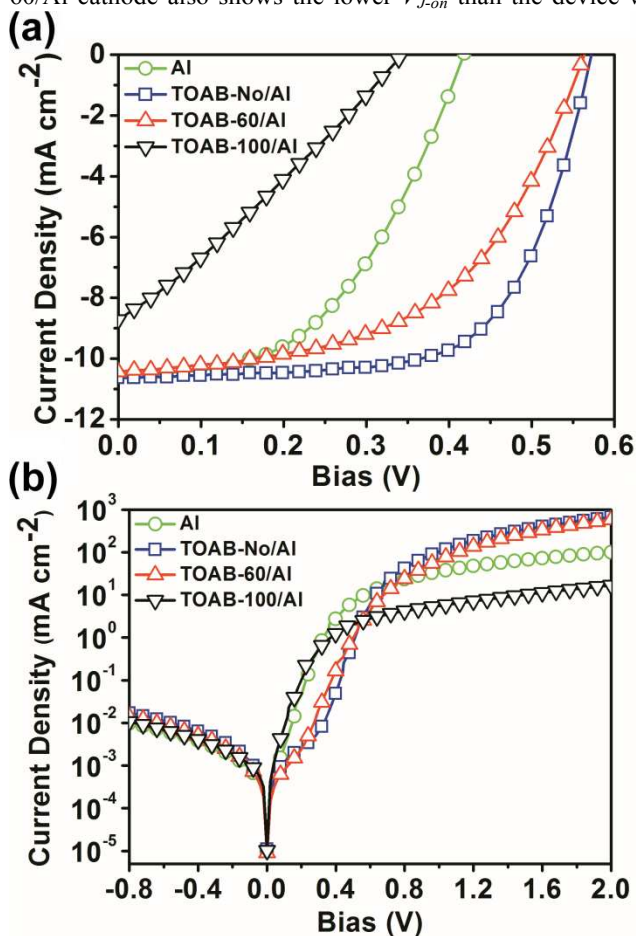


Fig. 8 J - V characteristics of PSCs with Al, TOAB-No/Al,

Conclusions

We clearly demonstrate the significance of ions with an ordered arrangement for enhancing the electron injection/extraction in polymer optoelectronic devices by using the model compound of TOAB. The active layers of PLEDs and PSCs are well covered with TOAB-No and TOAB-100, but poorly covered with TOAB-60 due to the formation of large islands. There are crystals possessing the (002) lattice planes parallel to the surface of the active layers in TOAB-No and TOAB-60 while the amorphous TOAB-100 is observed. Despite the very different surface morphology of TOAB-No and TOAB-60, the electron injection in PLEDs and the electron extraction in PSCs are significantly enhanced using TOAB-No and TOAB-60. On the other hand, the amorphous TOAB-100 acts an insulator to block the electron injection/extraction at the active layer-cathode interface. Accordingly, the origin of the enhanced electron injection/extraction is attributable to the interfacial dipole introduced by the ordered arrangement between Br^- and N^+ . The interfacial dipole shifts the vacuum level at the active layer-cathode interface, therefore decreasing the barrier height for electron injection/extraction. Accordingly, we reason that with an ordered arrangement of ions, all ionic compounds should be excellent for enhancing the electron injection/extraction in polymer optoelectronic devices.

Experimental

ITO-coated glass substrates (RITEK Corp., $15 \Omega \square^{-1}$) were cleaned ultrasonically in detergent, deionized water, acetone, and isopropanol, sequentially, for 20 min each. Subsequently, they were treated with UV ozone for 25 min. PEDOT:PSS (ClevisTM P VP Al 4083) was spin-coated on each substrate at

4000 rpm for 60 s and then baked at 150°C for 30 min. To prepare the active layer in PLEDs, the toluene solution of G-PF (Dow Chemical Corp.) with a concentration of 10 mg ml⁻¹ was spin-coated atop PEDOT:PSS at 2500 rpm for 60 sec and then baked at 65°C for 30 min. On the other hand, the active layer in PSCs (P3HT:PCBM) was obtained by the slow-growth process without any heat treating.²⁵ P3HT (Rieke Metals, Inc.) and PCBM (Nano-C, Inc.) were used as received. The P3HT:PCBM blend with the ratio of 1:1 w/w was dissolved in 1,2-dichlorobenzene (20:20 mg ml⁻¹) with a stir at least for 24 h in a nitrogen-filled glove box. After spin-coating the P3HT:PCBM solution atop PEDOT:PSS, the samples were dried in covered glass petri dishes. The annealing temperature was calibrated atop the TOAB layer by using a thermometer (YFE, YF-160A Type-K, Taiwan). The Al cathode of each device (80 nm) was thermally evaporated at a pressure about 10⁻⁶ torr. The area of each device was 0.06 cm² defined by a shadow mask during thermal evaporation of the Al cathode.

The *J-V* characteristics of PLEDs were measured by using a Keithley 2400 source-measure unit. The luminance of PLEDs was measured by using a calibrated Si-photodiode along with a Keithley 2000 digital multimeter and then calibrated by using a Minolta LS-100 luminance meter. The *J-V* characteristics of PSCs under an AM 1.5 G illumination of 100 mW cm⁻² and in the dark were measured by using a Keithley 2400 source-measure unit. The AM 1.5 G illumination was simulated by using an Oriel 91160A 300 W Solar Simulator and calibrated by a standard Si photodiode detector with a KG-5 color filter (Hammastau, S1133).⁴⁰ The R_S values were calculated from the reciprocal slope at 2.0 V in the dark *J-V* characteristics of devices.⁴¹ The measurement for PLEDs and PSCs was carried out in a nitrogen-filled glove box.

XRD experiments were performed using the X-ray with a wavelength of 1.0252 Å at the superconducting wiggler beamline BL13A1 of the National Synchrotron Radiation Research Center (NSRRC), Taiwan. The grain sizes of TOAB and P3HT were estimated by the full width at half maximum of the diffraction peak. AFM topography/phase images were obtained by a NanoScope IIIa (Digital instrument Inc.) operating in the tapping mode. The coverage of TOAB-60 atop G-PF was estimated by ImageJ.

Acknowledgements

Financial support by the National Science Council (NSC), Taiwan, (NSC 100-2221-E-006-165-MY2 and NSC 101-2918-I-006-022) is gratefully acknowledged. Technical support by both beamlines BL13A1 and BL17B1 of NSRRC, Taiwan, is also acknowledged.

Notes and references

^a Department of Chemical Engineering, National Cheng Kung University, Tainan 70101, Taiwan. E-mail: tcwen@mail.ncku.edu.tw

^b Department of Engineering and System Science, National Tsing-Hua University, Hsinchu 30013, Taiwan.

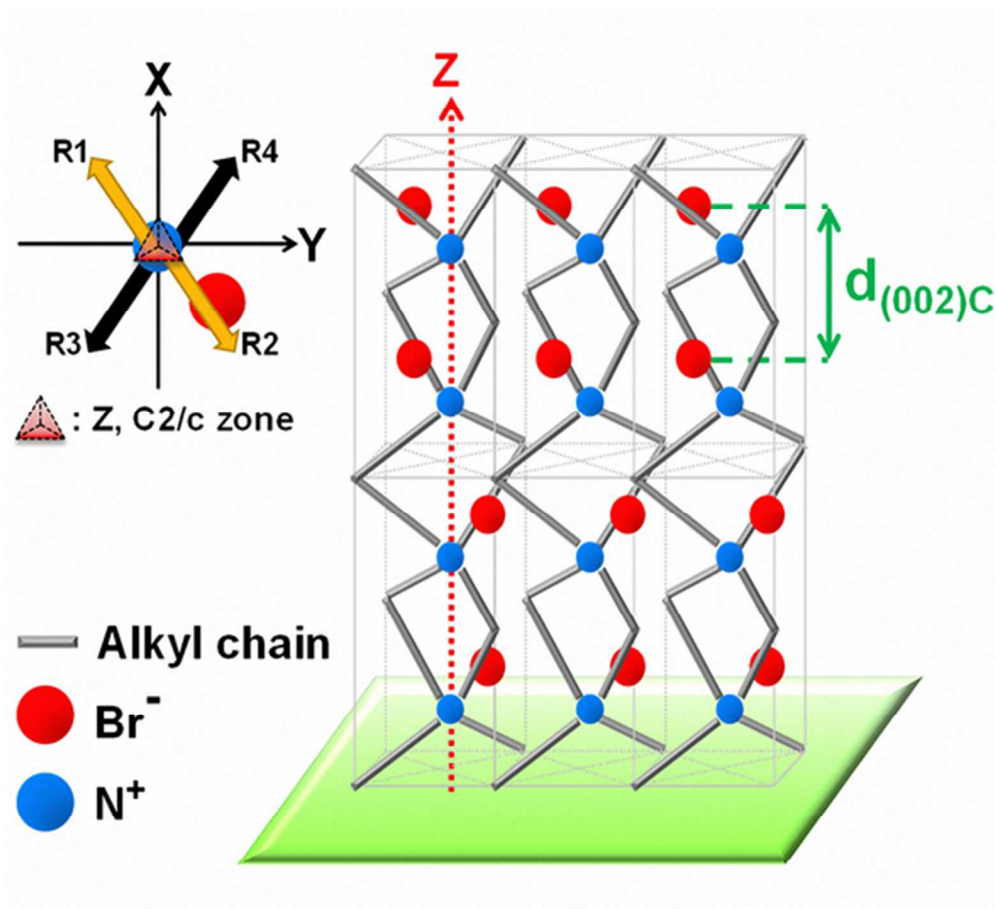
^c Department of Photonics, National Cheng Kung University, Tainan 70101, Taiwan.

^d Advanced Optoelectronic Technology Center, National Cheng Kung University, Tainan 70101, Taiwan.

^e Department of Materials Science and Engineering, University of Washington, Seattle, Washington 98195, USA.

- J. H. Burroughes, D. D. C. Bradley, A. R. Brown, R. N. Marks, K. Mackay, R. H. Friend, P. L. Burns and A. B. Holmes, *Nature*, 1990, **347**, 539.
- G. Yu, J. Gao, J. C. Hummelen, F. Wudl and A. J. Heeger, *Science*, 1995, **270**, 1789.
- H. Ma, H. L. Yip, F. Huang and A. K. Y. Jen, *Adv. Funct. Mater.*, 2010, **20**, 1371.
- L. M. Chen, Z. Xu, Z. R. Hong and Y. Yang, *J. Mater. Chem.*, 2010, **20**, 2575.
- H. L. Yip and A. K. Y. Jen, *Energy Environ. Sci.*, 2012, **5**, 5994.
- F. Huang, H. B. Wu and Y. Cao, *Chem. Soc. Rev.*, 2010, **39**, 2500.
- A. Duarte, K. Y. Pu, B. Liu and G. C. Bazan, *Chem. Mater.*, 2011, **23**, 501.
- J. H. Seo, A. Gutacker, Y. M. Sun, H. B. Wu, F. Huang, Y. Cao, U. Scherf, A. J. Heeger and G. C. Bazan, *J. Am. Chem. Soc.*, 2011, **133**, 8416.
- H. Jiang, P. Taranekekar, J. R. Reynolds and K. S. Schanze, *Angew. Chem., Int. Ed.*, 2009, **48**, 4300.
- J. Park, R. Q. Yang, C. V. Hoven, A. Garcia, D. A. Fischer, T. Q. Nguyen, G. C. Bazan and D. M. DeLongchamp, *Adv. Mater.*, 2008, **20**, 2491.
- C. Hoven, R. Yang, A. Garcia, A. J. Heeger, T. Q. Nguyen and G. C. Bazan, *J. Am. Chem. Soc.*, 2007, **129**, 10976.
- C. V. Hoven, R. Q. Yang, A. Garcia, V. Crockett, A. J. Heeger, G. C. Bazan and T. Q. Nguyen, *Proc. Natl. Acad. Sci. U. S. A.*, 2008, **105**, 12730.
- A. Garcia, R. C. Bakus, P. Zalar, C. V. Hoven, J. Z. Brzezinski and T. Q. Nguyen, *J. Am. Chem. Soc.*, 2011, **133**, 2492.
- C. H. Duan, L. Wang, K. Zhang, X. Guan and F. Huang, *Adv. Mater.*, 2011, **23**, 1665.
- J. F. Fang, B. H. Wallikewitz, F. Gao, G. L. Tu, C. Muller, G. Pace, R. H. Friend and W. T. S. Huck, *J. Am. Chem. Soc.*, 2011, **133**, 683.
- X. Guan, K. Zhang, F. Huang, G. C. Bazan and Y. Cao, *Adv. Funct. Mater.*, 2012, **22**, 2846.
- F. Liu, Z. A. Page, V. V. Duzhko, T. P. Russell and T. Emrick, *Adv. Mater.*, 2013, **25**, 6868.
- C. H. Duan, K. Zhang, X. Guan, C. M. Zhong, H. M. Xie, F. Huang, J. W. Chen, J. B. Peng and Y. Cao, *Chem. Sci.*, 2013, **4**, 1298.
- C. Min, C. S. Shi, W. J. Zhang, T. G. Jiu, J. S. Chen, D. G. Ma and J. F. Fang, *Angew. Chem., Int. Ed.*, 2013, **52**, 3417.
- S. N. Hsieh, S. W. Hsiao, T. Y. Chen, C. Y. Li, C. H. Lee, T. F. Guo, Y. J. Hsu, T. L. Lin, Y. Wei and T. C. Wen, *J. Mater. Chem.*, 2011, **21**, 8715.
- C. H. Wu, C. Y. Chin, T. Y. Chen, S. N. Hsieh, C. H. Lee, T. F. Guo, A. K. Y. Jen and T. C. Wen, *J. Mater. Chem. A*, 2013, **1**, 2582.
- D. J. Abdallah, R. E. Bachman, J. Perlstein and R. G. Weiss, *J. Phys. Chem. B*, 1999, **103**, 9269.
- A. Xenopoulos, J. Cheng, M. Yasuniwa and B. Wunderlich, *Mol. Cryst. Liq. Cryst.*, 1992, **214**, 63.
- Y. F. Chang, C. Y. Chen, F. T. Luo, Y. C. Chao, H. F. Meng, H. W. Zan, H. W. Lin, S. F. Horng, T. C. Chao, H. C. Yeh and M. R. Tseng, *Org. Electron.*, 2012, **13**, 388.

- 25 G. Li, V. Shrotriya, J. S. Huang, Y. Yao, T. Moriarty, K. Emery and Y. Yang, *Nat. Mater.*, 2005, **4**, 864.
- 26 P. Damman, S. Gabriele, S. Coppee, S. Desprez, D. Villers, T. Vilmin, E. Raphael, M. Hamieh, S. Al Akhrass and G. Reiter, *Phys. Rev. Lett.*, 2007, **99**, 036101.
- 27 H. Ishii, K. Sugiyama, E. Ito and K. Seki, *Adv. Mater.*, 1999, **11**, 605.
- 28 F. J. J. Janssen, L. J. van IJzendoorn, A. W. D. van der Gon, M. J. A. de Voigt and H. H. Brongersma, *Phys. Rev. B*, 2004, **70**, 165425.
- 29 J. A. Geddes and C. A. Kraus, *Trans. Faraday Soc.*, 1936, **32**, 585.
- 30 H. P. Li, Y. H. Xu, C. V. Hoven, C. Z. Li, J. H. Seo and G. C. Bazan, *J. Am. Chem. Soc.*, 2009, **131**, 8903.
- 31 R. Q. Yang, Y. H. Xu, X. D. Dang, T. Q. Nguyen, Y. Cao and G. C. Bazan, *J. Am. Chem. Soc.*, 2008, **130**, 3282.
- 32 G. Liu, A. Y. Li, D. An, H. B. Wu, X. H. Zhu, Y. Li, X. R. Miao, W. L. Deng, W. Yang, Y. Cao and J. Roncali, *Macromol. Rapid Commun.*, 2009, **30**, 1484.
- 33 P. Zalar, T. V. Pho, A. Garcia, B. Walker, W. Walker, F. Wudl and T. Q. Nguyen, *J. Phys. Chem. C*, 2011, **115**, 17533.
- 34 G. Liu, Y. H. Li, W. Y. Tan, Z. C. He, X. T. Wang, C. Zhang, Y. Q. Mo, X. H. Zhu, J. B. Peng and Y. Cao, *Chem.-Asian J.*, 2012, **7**, 2126.
- 35 W. L. Ma, C. Y. Yang, X. Gong, K. Lee and A. J. Heeger, *Adv. Funct. Mater.*, 2005, **15**, 1617.
- 36 Y. F. Li, *Acc. Chem. Res.*, 2012, **45**, 723.
- 37 G. G. Malliaras, J. R. Salem, P. J. Brock and J. C. Scott, *J. Appl. Phys.*, 1998, **84**, 1583.
- 38 J. Liu, Y. J. Shi, L. P. Ma and Y. Yang, *J. Appl. Phys.*, 2000, **88**, 605.
- 39 A. Hayakawa, O. Yoshikawa, T. Fujieda, K. Uehara and S. Yoshikawaa, *Appl. Phys. Lett.*, 2007, **90**, 163517.
- 40 V. Shrotriya, G. Li, Y. Yao, T. Moriarty, K. Emery and Y. Yang, *Adv. Funct. Mater.*, 2006, **16**, 2016.
- 41 C. Waldauf, M. C. Scharber, P. Schilinsky, J. A. Hauch and C. J. Brabec, *J. Appl. Phys.*, 2006, **99**, 104503.



The ordered arrangement of ions contributes to the enhanced electron injection/extraction in polymer optoelectronic devices and can be manipulated by adequate thermal annealing treatment.
50x45mm (300 x 300 DPI)